RESEARCH

Singular adaptations in the carbon assimilation mechanism of the polyextremophile cyanobacterium *Chroococcidiopsis thermalis*

Pere Aguiló-Nicolau[1] · Jeroni Galmés[1] · Giacomo Fais[2] · Sebastià Capó-Bauçà[1] · Giacomo Cao[2,3] · Concepción Iñiguez[1]

Abstract

Cyanobacteria largely contribute to the biogeochemical carbon cycle fixing ~ 25% of the inorganic carbon on Earth. However, the carbon acquisition and assimilation mechanisms in Cyanobacteria are still underexplored regardless of being of great importance for shedding light on the origins of autotropism on Earth and providing new bioengineering tools for crop yield improvement. Here, we fully characterized these mechanisms from the polyextremophile cyanobacterium *Chroococcidiopsis thermalis* KOMAREK 1964/111 in comparison with the model cyanobacterial strain, *Synechococcus* sp. PCC6301. In particular, we analyzed the Rubisco kinetics along with the in vivo photosynthetic CO_2 assimilation in response to external dissolved inorganic carbon, the effect of CO_2 concentrating mechanism (CCM) inhibitors on net photosynthesis and the anatomical particularities of their carboxysomes when grown under either ambient air (0.04% CO_2) or 2.5% CO_2-enriched air. Our results show that Rubisco from *C. thermalis* possess the highest specificity factor and carboxylation efficiency ever reported for Cyanobacteria, which were accompanied by a highly effective CCM, concentrating CO_2 around Rubisco more than 140-times the external CO_2 levels, when grown under ambient CO_2 conditions. Our findings provide new insights into the Rubisco kinetics of Cyanobacteria, suggesting that improved $S_{c/o}$ values can still be compatible with a fast-catalyzing enzyme. The combination of Rubisco kinetics and CCM effectiveness in *C. thermalis* relative to other cyanobacterial species might indicate that the co-evolution between Rubisco and CCMs in Cyanobacteria is not as constrained as in other phylogenetic groups.

Keywords Cyanobacteria · Rubisco · CO_2-concentrating mechanisms · CO_2-fixation · Photosynthesis

Introduction

Cyanobacteria is one of the most primitive life forms on Earth (Knoll 2008). With the appearance of oxygenic photosynthesis more than 2500 Mya, cyanobacterial metabolism changed the composition of the primitive atmosphere, rising oxygen levels with the consequent decrease in CO_2 (Blank 2013; Schirrmeister et al. 2016; Sánchez-Baracaldo et al. 2022). Atmospheric oxygen rise permitted the evolution of a more complex life, leading to the large biological variability found in the present (Dismukes et al. 2001). Nowadays, the photosynthetic activity of Cyanobacteria makes an important contribution to the biosphere carbon cycle, with recent estimations indicating that it represents more than 25% of the total CO_2 fixation on Earth (Rae et al. 2013). Cyanobacteria occupy a wide variety of habitats such as terrestrial, marine, brackish-water, freshwater, and even extreme environments (Tomitani et al. 2006). However, the carbon acquisition and assimilation mechanisms of the diverse cyanobacterial group have been barely studied, and research has only been focused on a few model cyanobacterial species (Espie and Kimber 2011; Whitehead et al. 2014; Xia et al. 2020; Basu and Mackey 2022).

✉ Jeroni Galmés
jeroni.galmes@uib.cat

1   Research Group on Plant Biology Under Mediterranean Conditions, Universitat de les Illes Balears, INAGEA, Ctra. Valldemossa km. 7.5, 07122 Palma, Balearic Islands, Spain

2   Interdepartmental Centre of Environmental Science and Engineering, University of Cagliari, Via San Giorgio 12, 09124 Cagliari, Italy

3   Department of Mechanical, Chemical and Materials Engineering, University of Cagliari, Via Marengo 2, 09123 Cagliari, Italy

The ultimate responsible of the inorganic carbon fixation in photosynthetic organisms is the enzyme Ribulose-1,5-bisphosphate carboxylase/oxygenase (Rubisco, EC 4.1.1.39) (Spreitzer and Salvucci 2002). Besides its carboxylating activity, Rubisco also catalyzes the oxygenation of Ribulose-1,5-bisphosphate (RuBP), leading to the photorespiration pathway, which consumes energy and leads to inorganic carbon loss (Hamilton 2019). Other two catalytic particularities of Rubisco are its relatively poor affinity for CO_2 and low carboxylation turnover rate (k_{cat}^c) (Galmés et al. 2014b). These catalytic limitations of Rubisco constrain the CO_2 assimilation capacity of photosynthetic organisms and, under stressful conditions, it may even compromise achieving sufficient rates of inorganic carbon fixation to support autotropism (Bauwe et al. 2010, 2012). Three different adaptive mechanisms have been described to occur in photosynthetic organisms that allow them to counterbalance Rubisco catalytic limitations: (i) increasing Rubisco concentration, (ii) increasing CO_2 concentration at the active sites of Rubisco, and (iii) optimizing Rubisco kinetics to the intracellular concentrations of the two gaseous substrates, CO_2 and O_2 (Flamholz and Shih 2020).

Rubisco constitutes the most abundant enzyme on Earth, being up to 50% of the total soluble protein in C_3 plant leaves (Ellis 1979; Spreitzer and Salvucci 2002). Nevertheless, there is a large variability in Rubisco content among photosynthetic organisms, which is linked to nutrient (especially nitrogen) and CO_2 availability (Andersson and Backlund 2008). For example, higher amounts of the enzyme have been found in organisms that depend on the diffusive CO_2 entry from the atmosphere to the sites of carboxylation (Raven 2013). On the contrary, other organisms evolved mechanisms that increase CO_2 around Rubisco active sites, i.e., the so-called CO_2 concentrating mechanisms (CCMs), which lead to a lower Rubisco content (Losh et al. 2013). One example of the latter is Cyanobacteria, where Rubisco only accounts for 2 to 10% of the total soluble protein (Dai et al. 2018). The organisms presenting CCMs are C_4 and CAM terrestrial vascular plants, seagrasses, algae, Cyanobacteria, and some proteobacteria (Iñiguez et al. 2020; Capó-Bauçà et al. 2022b). Two types of CCMs have been described, biochemical and biophysical. The former involves a CO_2 fixation prior to that catalyzed by Rubisco (C_4 and CAM plants), and the latter involves the active transport of HCO_3^-/CO_2 across membranes and/or an increase in the external CO_2 concentration by acidification of the extracellular environment (aquatic organisms, i.e.: seagrasses, algae, Cyanobacteria, and Proteobacteria; Giordano et al. 2005). Cyanobacteria and some proteobacteria have evolved a particular CCM component consisting of a proteic polyhedral shell filled with Rubisco and carbonic anhydrase (CA), called carboxysome (Whitehead et al. 2014). HCO_3^- is actively accumulated in the cytosol, where there is no CA

activity, and enters the carboxysome, where CA catalyzes the dehydration of HCO_3^- to CO_2 and increases the CO_2 concentration around Rubisco, therefore enhancing carboxylation over oxygenation (Mangan and Brenner 2014; Mangan et al. 2016). This prokaryotic type of CCM is one of the most efficient inorganic carbon acquisition mechanisms, concentrating CO_2 around Rubisco active sites up to 100 times the extracellular CO_2 levels (Badger and Andrews 1987).

Regarding the optimization of Rubisco kinetics, a large variability in the main kinetic parameters has been observed across photosynthetic organisms (Young et al. 2016; Bathellier et al. 2018; Flamholz et al. 2019; Iñiguez et al. 2020). The highest values of CO_2/O_2 specificity ($S_{c/o}$; up to 240 mol mol^{-1}) and the highest affinities for CO_2 (which means the lowest Michaelis–Menten semi-saturation constant for CO_2 measured at 0% O_2, K_c; down to 3.3 μM) are found in Rhodophyta (Whitney et al. 2001), whereas the highest Rubisco carboxylation turnover rates (k_{cat}^c) are found in Proteobacteria (up to 22.2 s^{-1}, Davidi et al. 2020). However, the vast majority of the Rubisco kinetic data to date belongs to higher plants, implying an important bias towards other phylogenetic groups (Flamholz et al. 2019; Iñiguez et al. 2020). Large variability in Rubisco kinetics has been observed in the few cyanobacterial strains analyzed so far, with $S_{c/o}$ values ranging between 32 and 60 mol mol^{-1}; K_c ranging between 80 and 309 μM, the Michaelis–Menten semi-saturation constant for O_2 (K_o) ranging between 529 and 1400 μM, and k_{cat}^c ranging between 2.41 and 14.4 s^{-1} (Iñiguez et al. 2020). By contrast, in higher plants, $S_{c/o}$ values range from 60 to 120 mol mol^{-1}, K_c from 6 to 44 μM, K_o from 150 to 1500 μM, and k_{cat}^c from 1 to 7 s^{-1}.

The three variables described above that determine the carbon fixation capacity of an autotrophic organism (Rubisco concentration, CO_2 concentration at the sites of Rubisco carboxylation, and Rubisco kinetics) are not independent of each other, and it is believed that they have co-evolved shaped by both phylogeny and environment (Galmés et al. 2014a; Tcherkez et al. 2018). For example, the presence of CCMs in terrestrial vascular plants is correlated with a lower Rubisco content and an enhancement of k_{cat}^c at the expense of a loss in Rubisco affinity for CO_2 (higher K_c) (Galmés et al. 2014b). However, the co-evolution of Rubisco kinetics and CCMs have only been widely investigated in higher plants, leaving other phylogenetic groups, such as Cyanobacteria, understudied. In addition, extremophile organisms present specific adaptations to optimize carbon fixation under unfavorable conditions; therefore, one question that remains to be answered is whether the analysis of extremophile cyanobacteria could widen the range of variability of Rubisco kinetics and CCM operation found in the previously analyzed model species.

To answer if extremophile cyanobacteria could possess singular adaptations in the carbon acquisition and assimilation mechanisms, we performed a complete analysis on Rubisco kinetics, operation of inorganic carbon acquisition mechanisms, CCM effectiveness and anatomical imaging of *Chroococcidiopsis thermalis* KOMAREK 1964/111, a polyextremophile cyanobacterium inhabiting desertic rock surfaces, supporting temperatures up to 50 °C, high UV radiation and desiccation (Billi et al. 2011; Cumbers and Rothschild 2014); in comparison with the model species *Synechococcus* sp. PCC6301. We hypothesize that *C. thermalis* has evolved multiple mechanisms that allowed its adaptation to a wide range of CO_2 conditions derived from the harsh environments where this cyanobacterium inhabits.

Materials and methods

Cyanobacterial cultures

Cyanobacterial strains of *Synechococcus* sp. (PCC 6301/UTEX 625; CCALA 188) and *Chroococcidiopsis thermalis* (KOMAREK 1964/111; CCALA 048) were acquired from the Culture Collection of Autotrophic Organisms (CCALA, Třeboň, Czech Republic). *Synechococcus* sp. was grown in 1 L sterilized flasks under orbital agitation, and *C. thermalis* was grown in 140 mm × 20 mm glass Petri dishes without agitation. Both cultures were maintained in Z-medium (Staub 1961) at 20 °C in a 16:8 light–dark cycle with a light intensity of 50 μmol m^{-2} s^{-1} for *Synechococcus* sp. and 30 μmol m^{-2} s^{-1} for *C. thermalis* (according to their optimum growth irradiances) provided by a cool-white light source (4000 K; Osram L 18W/840 Lumilux, Germany), in a temperature-controlled chamber (Aralab Fitoclima S600 PLH, Spain). Growth rate was followed by spectrophotometry at 650 nm (OD_{650}, Thermo scientific Multiskan Sky 1530-00433C, USA). When cultures reached an OD650 value of 0.4, control and enriched CO_2 experiments were started, each with three autoclaved flasks of 100 mL culture connected to a constant air-flux of 5 mL/min of either ambient air (0.04% CO_2, LC) or 2.5% CO_2-enriched air (HC), respectively. Both species were grown under constant agitation during the experiment and maintained in exponential growth phase. After 7–10 days of acclimation to the two CO_2 treatments, the physiological measurements described below were done.

O$_2$ evolution measurements

Net photosynthesis and the effect of external and internal carbonic anhydrases (CAs) and anion-exchange bicarbonate transporter inhibitors on net photosynthesis were determined at the culture temperature (20 °C) by monitoring O_2 evolution using Clark-type oxygen electrode chambers (Oxygraph, Hansatech, UK). 2 mL of culture were placed in the chamber, illuminated with white-light LED lamps at a saturating photosynthetic irradiance [300 μmol m^{-2} s^{-1}, previously determined for both species by chlorophyll *a* fluorescence light curves using a pulse-amplitude-modulated fluorometer (Dual-PAM-100, Walz, Germany)]. O_2 evolution rates were taken at 2–3 min intervals after rate stabilization, using the O2view software (version 2.10, Hansatech). Rates were normalized to the dry weight (DW) of biomass, which was obtained weighing the dried 2 mL pellet of each measurement.

To assess the role of CAs in photosynthesis, the percentage of net photosynthesis inhibition after adding 200 μM of acetazolamide (AZ, external CAs inhibitor) and 200 μM of ethoxyzolamide (EZ, external and internal CAs inhibitor) was monitored. The same procedure was followed after adding 300 μM of the anion-exchange transporter inhibitor 4,4′-diisothiocyanatostilbene-2,2′-disulfonate (DIDS) to a fresh 2 mL culture aliquot.

Photosynthesis-dissolved inorganic carbon (DIC) curves were done at saturating photosynthetic irradiance (300 μmol m^{-2} s^{-1}) at 25 °C to be able to compare the obtained in vivo carbon fixation rates with those from in vitro Rubisco measurements (also done at the standard temperature of 25 °C). 2 mL fresh culture was washed three times with CO_2 free-Z medium with 20 mM Tris–HCl (pH 8), by gentle centrifugation (3000×*g* for 3 min). Initial O_2 concentration inside the chambers was lowered to 70% by bubbling with N_2 to avoid O_2 oversaturation during the curve. Oxygen saturation in air-equilibrated media was determined using DOTABLES (https://water.usgs.gov/software/DOTABLES/) software for the specific conductivity of the medium at 25 °C. After zero net photosynthesis was detected, increasing concentrations of DIC were added every 2–3 min, obtaining rates for 8–12 different DIC concentrations in the chamber (0–1500 μM for LC-grown cells and 0–5000 μM for HC-grown cells). Dissolved CO_2 concentration in equilibrium in the medium for each DIC concentration assayed was calculated using CO2sys software and curves were fitted to the Michaelis–Menten equation obtaining the maximum photosynthetic rate (A_{max}) and the in vivo photosynthetic semi-saturation constant for CO_2 ($K_{m\ in\ vivo}$).

Carbon isotopic discrimination

The ^{13}C isotopic discrimination in cyanobacterial cells was obtained from a 50 mL culture aliquot at OD_{650} of 0.8–1, which was centrifuged at 10,000×*g* for 3 min. The pellet was freeze-dried overnight and homogenized. 0.2 g of the dried powder was transferred into metallic capsules (176980926, Lüdiswiss, Switzerland) and combusted in an elemental analyzer (Thermo Flash EA 1112 Series, Germany) where

CO_2 was injected into a continuous-flow isotope mass spectrometer (Thermo-Finnigan Delta XP, Bremen, Germany). Peach leaf standards (NIST 1547) were measured every six samples. Results are presented as δ vs. PDB (Pee Dee Belemnite). The obtained ^{13}C isotopic discrimination of the cyanobacterial biomass ($δ^{13}C$) was corrected with the ^{13}C isotopic composition of DIC found in the medium from either CO_2-enriched or control experiments, as described by Iñiguez et al. (2016).

Total soluble proteins and Rubisco quantification

50 mL culture aliquots at OD_{650} of 0.8–1 were centrifuged at $10,000 \times g$ for 3 min. Pellets were immediately frozen in liquid nitrogen and homogenized in a mixer mill (Retsch GmbH MM200) with 2 mL cold Extraction Buffer containing 100 mM EPPS (pH 8.1), 1 mM ethylenediamine-tetraacetic acid (EDTA), 20 mM $MgCl_2$, 2% CelLytic™ B (B7435, Sigma-Aldrich), 1 M dithiothreitol (DTT), 2% plant protease inhibitor cocktail (P9599, Merck, USA), 100 mM β-mercaptoethanol and 0.1 g polyvinylpolypyrrolidone (PVPP). The homogenate was then centrifuged for 5 min at $3000 \times g$ at 4 °C. The supernatant was kept on ice and the pellet was frozen in liquid nitrogen and milled again. This process was repeated three times to ensure maximum extraction efficiency.

A supernatant aliquot was used to quantify the total soluble protein (TSP) content following Bradford's (1976) method, and to quantify Rubisco content by Western blot immunodetection of the Rubisco large subunit using purified Rubisco standard and Rubisco large subunit antibody (AS01 017S and AS03 037 Agrisera, Sweden) at 1:20,000 dilution and Goat anti-Rabbit IgG HRP-conjugated secondary antibody (AS09 602 Agrisera, Sweden) at 1:50,000 dilution (see Supplementary Fig. 2).

Rubisco catalytic measurements

The previously described crude protein extract was partially purified using a 5 mL Mini-Macroprep High-Q strong anion-exchange cartridge (Bio-Scale Mini Macro-Prep High Q Cartridge 7324124, Bio-Rad, USA) and then desalted and concentrated ~ tenfold using Amicon Ultra 4 (Z740198, Merck, USA) by centrifuging at $1000 \times g$ at 4 °C. Rubisco carboxylation kinetic traits were determined at 25 °C as explained in (Capó-Bauçà et al. 2020) 7 mL-septum capped crystal vials with magnetic stirrer containing 400 μL of Assay Buffer (100 mM Bicine (pH 8.1), 20 mM $MgCl_2$) and ~ 100 W-A units of carbonic anhydrase (C3934 Merck, USA) were bubbled with 100% N_2 gas or CO_2-free synthetic air (21% O_2, 79% N_2) for 2 h. After that, one of eight different concentrations of $NaH^{14}CO_3$ from 0 to 60 mM with a specific activity of 3.7×10^{10} Bq

mol^{-1} and 1.6 mM of RuBP [synthesized and purified as explained in Kane et al. (1994)] were added to each vial. The semi-purified protein extracts were supplemented with 20 mM $NaH^{14}CO_3$ and pre-activated for 30 min at 35 °C (optimum incubation time and temperature for full Rubisco activation, as previously determined). Assays were started by adding 20 μL of preactivated extract and led to react for 1 min (final reaction volume of 0.495 mL). The reaction was stopped by adding 200 μL of 10 M formic acid and dried at 80 °C. Non-volatile acid-stable ^{14}C-organic molecules were determined by scintillation counting (Beckman Coulter LS6500, USA).

The semi-saturation constant for CO_2 under 0% and 21% O_2 (K_c and $K_c^{21\% O_2}$, respectively) and the maximum carboxylation velocity (V_{max}^c) were determined from fitting the data to the Michaelis–Menten equation. The semi-saturation constant for O_2 (K_o) was calculated in each biological replicate by a linear fit of K_c measurements obtained under 0% and 21% O_2. CO_2 concentration in solution was calculated assuming a carbonic acid dissociation constant (pK_a) of 6.11 at 25 °C (Galmés et al. 2016) using accurate measurements of the assay buffer pH at 25 °C. k_{cat}^c was calculated by dividing V_{max}^c by Rubisco active site's concentration, the latter determined by incubating the same semi-purified protein extracts for 30 min at room temperature with 2′-carboxyarabinitol-1,5-bisphosphate (^{14}C-CABP) (Ruuska et al. 1998), assuming eight active binding sites per Rubisco (Blayney et al. 2011). The optimal concentration of ^{14}C-CABP for Rubisco quantification was determined for each cyanobacterial strain as explained in (Capó-Bauçà et al. 2022b).

Rubisco's specificity factor ($S_{c/o}$) was assayed with [1-^3H]RuBP as explained by Kane et al. (1994), using the same semi-purified extracts as for kinetics. 7 mL septum-capped crystal vials containing 940 μL of Assay buffer (30 mM Triethanolamine-acetate (pH 8.3) and 15 mM Mg-acetate), 400 W-A units of carbonic anhydrase and 20 μL of semi-purified protein extract were bubbled with a gas mixture of 99.95% O_2 and 0.05% CO_2 for 1 h. The reaction was initiated by adding ~ 1 nmol of [1-^3H] RuBP and incubated for 1 h at 25 °C with continuous stirring (final reaction volume of 1 mL). The reaction was stopped by adding 0.35 U of alkaline phosphatase (P7640, Merck, USA). The reaction product was purified using anion exchange AG1-X8 resin (1401441, Bio-Rad, USA), and then, glycolate and glycerate picks were separated by high-performance liquid chromatography (HPLC; Jasco-UV-4075, Jasco inc., USA) and quantified by scintillation counting (Beckman Coulter LS6500, USA). $S_{c/o}$ was calculated using a CO_2/O_2 solubility ratio of 0.038 at 25 °C.

Rubisco kinetic parameters obtained in the present study for *Synechococcus* sp. and *C. thermalis* were

compared to all cyanobacterial Rubisco kinetic data available to date. These data were extracted from the compilation of Iñiguez et al. (2020), which includes Rubisco kinetic data from phylogenetically distant organisms (see Supplementary Spreadsheet 1).

Transmission electron microscope imaging

1 mL culture aliquots ($OD_{650} \sim 0.8$) were centrifuged at $10,000 \times g$. The pellet was then resuspended in 1 mL fixation buffer (0.1 M phosphate buffer pH 7.2, 4% glutaraldehyde, 2% paraformaldehyde) and stored at 4 °C under darkness. Post-fixation was performed in 1% osmium tetroxide, prepared in 0.1 M Sorensen's phosphate buffer, for 1 h. The fixed sections were then stained in 2% uranyl acetate, dehydrated in a graded ethanol series, and embedded in London Resin White (EMS, Hatfield, PA). Semithin (1 μm thick) and ultrathin (50 to 70 nm thick) sections were cut using an ultramicrotome (UC7/FC7; Leica, Germany). The semithin sections were mounted on glass slides and stained with epoxy tissue stain (EMS, Hatfield, PA). The ultrathin sections were mounted on copper grids and visualized using the transmission electron microscope Jeol JEM 1400 operating at 80 kV. Image analysis was done using ImageJ software (Wayne Rasband National Institutes of Health, version 2.3.0/1.53q).

Rubisco gross assimilation modeling

An adaptation of Farquhar's biochemical model (Farquhar et al. 1980) was applied to the in vitro measured Rubisco kinetic traits to calculate the Rubisco gross assimilation rate per catalytic site (A_{Rub}) at varying CO_2 partial pressure at the Rubisco active sites of *Synechococcus* sp. and *C. thermalis* in comparison with the Rubisco kinetic traits of a model C_3 crop species, *Triticum aestivum*, obtained from Iñiguez et al. (2020) (Eq. 1).

$$A_{Rub} = \frac{(C - \Gamma^*) \cdot k_{cat}^c \cdot RCS}{C + K_c \cdot \left(1 + \frac{O}{K_o}\right)} \tag{1}$$

where k_{cat}^c, K_c and K_o are the carboxylation turnover rate and the Michaelis–Menten semi-saturation constants for carboxylation and oxygenation, respectively, measured in vitro at 25 °C. C and O are the CO_2 and O_2 partial pressure at the Rubisco active sites which, in the case of CO_2, range between 10 and 20,000 ppm, and, in the case of O_2, partial pressure is assumed to be constant at 210,000 ppm. $\Gamma^* = 0.5$ $O/S_{c/o}$, where $S_{c/o}$ is the CO_2/O_2 specificity factor measured in vitro at 25 °C. RCS is the number of Rubisco catalytic sites which was set to 1 to obtain the Rubisco gross assimilation rate per catalytic site.

Statistical analysis

The significance of differences was tested using two-way ANOVA after normality (Anderson–Darling test) and homoscedasticity (Levene test) was corroborated. For data that do not meet normality and/or homoscedasticity, the Kruskal–Wallis test was used to test the significance of differences. Post hoc comparisons were done using the Tukey test or the Bonferroni correction, respectively. Student's t test, or Mann–Whitney–Wilcoxon test for non-parametric data, was used to compare means between two groups of data. P values below 0.05 were considered significant. Data were analyzed using R (version 3.2.3 and RStudio version 0.99.879) and plots were done using the ggPlot2 package (version 2.2.1).

Results

The singularity of Rubisco kinetics from *C. thermalis* among Cyanobacteria species

In vitro Rubisco kinetic parameters measured at 25 °C show significant differences between *Synechococcus* sp. and *C. thermalis*, except for k_{cat}^c (Supplementary Table 1). *Chroococcidiopsis thermalis* presented 40% higher $S_{c/o}$, 70% higher affinity for CO_2 (i.e. lower K_c), 85% lower affinity for O_2 (i.e. higher K_o), and 75% higher catalytic carboxylation efficiency (k_{cat}^c/K_c) than *Synechococcus* sp. In addition, when compared with previously measured cyanobacterial Rubisco, *C. thermalis* possessed the most extreme values for most of the Rubisco kinetic parameters (Fig. 1). The highest value ever reported for $S_{c/o}$ in Cyanobacteria corresponded to *C. thermalis* (69.0 mol mol^{-1}) from the present study, being 1.4-fold higher than the cyanobacterial average (46.6 mol mol^{-1}) and twofold higher than the lowest values, observed in *Anabaena* sp. PCC7120 (35.0 mol mol^{-1}). The lowest values for K_c were found in *Aphanocapsa virescens* (Jordan and Ogren 1983) followed by *C. thermalis* (80.0 μM and 87.2 μM, respectively), both presenting the highest affinity for CO_2 among all measured cyanobacteria. This Rubisco affinity for CO_2 from *C. thermalis* was twofold higher than the cyanobacterial average, which means a twofold lower K_c than the average value of 167.78 μM for Cyanobacteria. When measured at 21% O_2, the Michaelis–Menten semi-saturation constant for CO_2 ($K_c^{21\% O_2}$) of *C. thermalis* was also the lowest among previously measured cyanobacteria (106.9 μM), followed by the hyperthermophile *Thermosynechococcus elongatus* BP-1 (107 μM; Wilson et al. 2018). This means that Rubisco CO_2 affinity under 21% O_2 in *C. thermalis* is more than twofold higher than the cyanobacterial average ($K_c^{21\% O_2}$ of 245.9 μM). Similar values of k_{cat}^c were obtained for *Synechococcus* sp. and *C. thermalis*
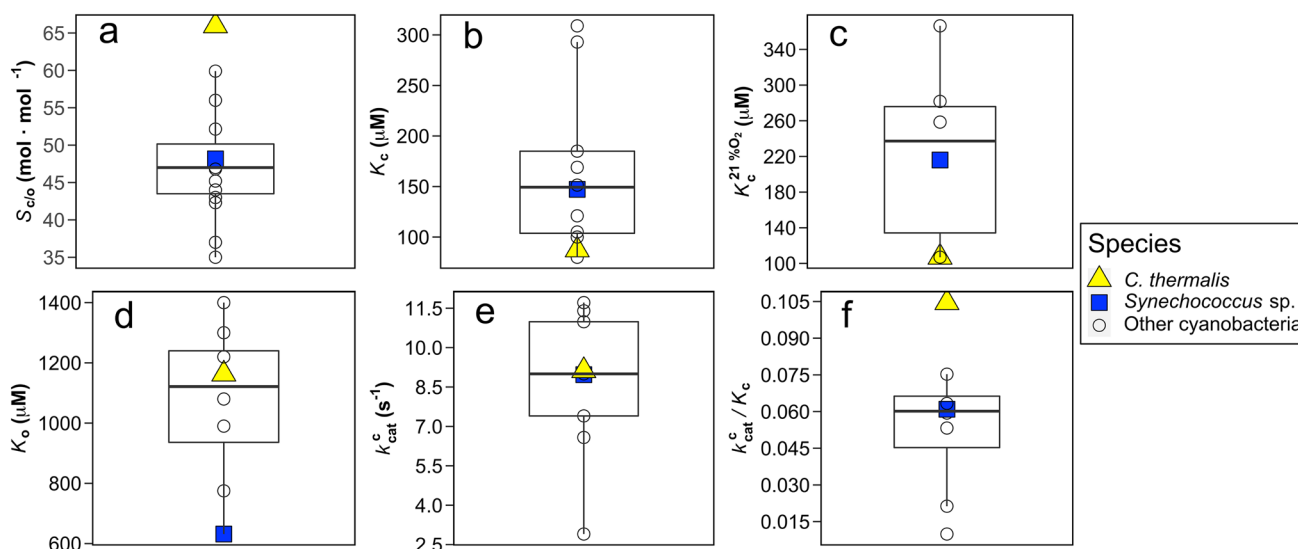
Fig. 1 In vitro Rubisco kinetic traits at 25 °C: **a** CO_2/O_2 specificity factor ($S_{c/o}$); **b** Michaelis–Menten semi-saturation constant for CO_2 at 0% O_2 (K_c); **c** Michaelis–Menten semi-saturation constant for CO_2 at 21% O_2 ($K_c^{21\% O_2}$); **d** Michaelis–Menten semi-saturation constant for O_2 (K_o); **e** carboxylation turnover rate (k_{cat}^c), and **f** Rubisco carboxylation efficiency (k_{cat}^c/K_c) of *Chroococcidiopsis thermalis* KOMAREK 1964/111 (yellow triangles) and *Synechococcus* sp. PCC6301 (blue squares), measured from semi-purified protein extracts of both strains

in the present study, compared to Rubisco kinetics of other previously measured cyanobacterial strains (data compilation from Iñiguez et al. 2020, empty circles). 3–6 replicates of each Rubisco kinetic parameter were used to calculate the mean value shown for *Synechococcus* sp. PCC6301 and *C. thermalis* KOMAREK 1964/111 in the boxplots (mean values and standard deviations are shown in Supplementary Table 1). For the other cyanobacterial strains, kinetic parameters are the mean of all values reported in the compiled studies for each strain (values and references provided in Supplementary Spreadsheet 1)

(9.0 s^{-1} and 9.1 s^{-1}, respectively) that fit the cyanobacterial average (k_{cat}^c of 9.8 s^{-1}). In addition, the highest value of k_{cat}^c/K_c ever reported for Cyanobacteria was found again in *C. thermalis* (0.10 s^{-1} μM), being more than twofold higher than the cyanobacterial average (0.05 s^{-1} μM). The lowest affinity for O_2 was observed in *Prochlorococcus marinus* MIT9313 (K_o of 1400 μM; Shih et al. 2016), whereas *C. thermalis* presented a relatively low affinity for O_2, with a K_o of 1163 μM.

Characterization and effectiveness of CO_2 concentrating mechanisms in *Synechococcus* sp. and *C. thermalis*

Net photosynthesis and effect of CCM inhibitors

Net photosynthetic rate (A_n) from *C. thermalis* and *Synechococcus* sp. under LC did not differ, averaging 47.7 μmol O_2 h^{-1} mg^{-1} DW. On the contrary, A_n from both species under HC (Fig. 2) showed significantly higher values for *Synechococcus* sp. than for *C. thermalis* (60.2 and 46.9 μmol O_2 h^{-1} mg^{-1} DW, respectively). Hence, the A_n of *Synechococcus* sp. under HC was higher than under LC, whereas no differences in A_n of *C. thermalis* were observed between CO_2 treatments.

In *Synechococcus* sp., A_n was significantly inhibited by the addition of AZ (which only inhibits external CAs) under

HC but not under LC, while in *C. thermalis*, A_n was inhibited by AZ in both CO_2 treatments (Table 1). *Chroococcidiopsis thermalis* showed a higher percentage of inhibition by AZ under HC than *Synechococcus* sp. (35.4% and 23.5% of net photosynthetic inhibition, respectively). In addition, A_n was strongly inhibited by the addition of EZ (which inhibits both internal and external CAs) in both species and CO_2 treatments (ranging from 47 to 87% inhibition), indicating the presence of constitutive internal CAs with an important contribution to net photosynthetic rate. The percentage of EZ inhibition in *C. thermalis* under HC was significantly higher than under LC (86.9% and 65.6%, respectively). No differences in the percentage of inhibition by EZ were observed between both species under LC, neither in *Synechococcus* sp. between HC and LC.

A_n of the two species in both CO_2 treatments was significantly inhibited by the addition of the anion-exchange transporter inhibitor DIDS, except for *C. thermalis* under LC (Table 1). A_n from *Synechococcus* sp. under HC was inhibited more than twofold by DIDS, in comparison with *C. thermalis* under HC (44.3 *vs.* 19.3% of inhibition). In addition, the percentage of DIDS inhibition in *Synechococcus* sp. under HC was significantly higher than under LC.
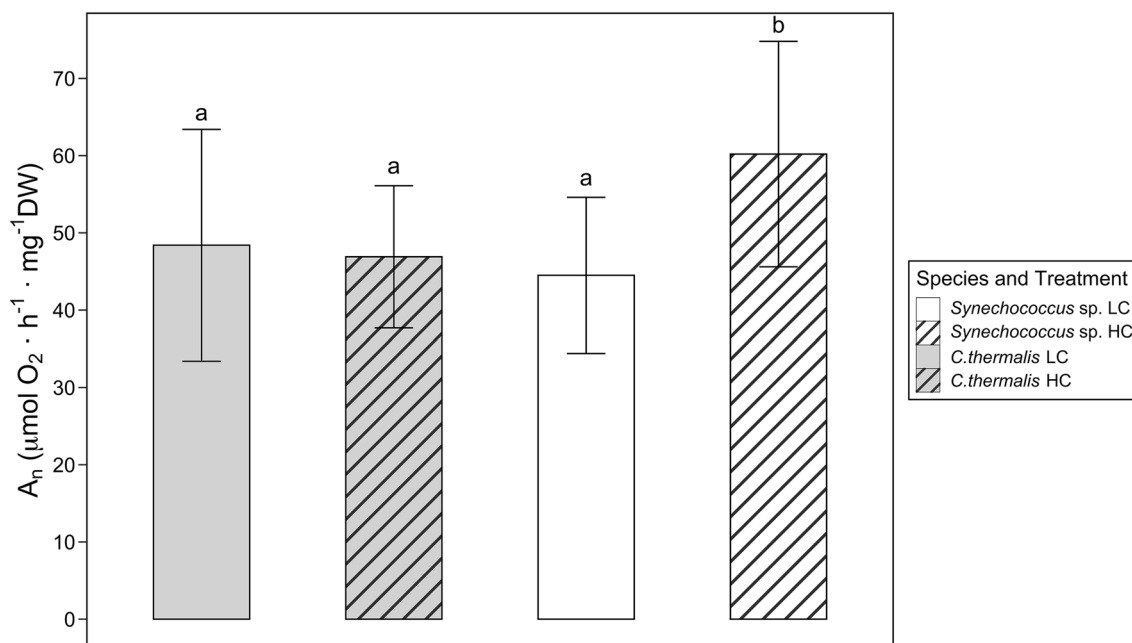
Fig. 2 Net photosynthetic rate (A_n) in *Synechococcus* sp. PCC6301 (white) and *Chroococcidiopsis thermalis* KOMAREK 1964/111 (grey) at 20 °C under ambient air (0.04% CO_2, LC, empty pattern) or 2.5% CO_2—enriched air (HC, line pattern) and saturating irradiance (300 µmol photons m^{-2} s^{-1}). Values are means ± standard deviation of 10 replicates. Different letters denote significant differences among different strains and CO_2 treatments ($P < 0.05$, two-way ANOVA followed by Tukey's test or Kruskal–Wallis test followed with Bonferroni correction for non-parametric data)
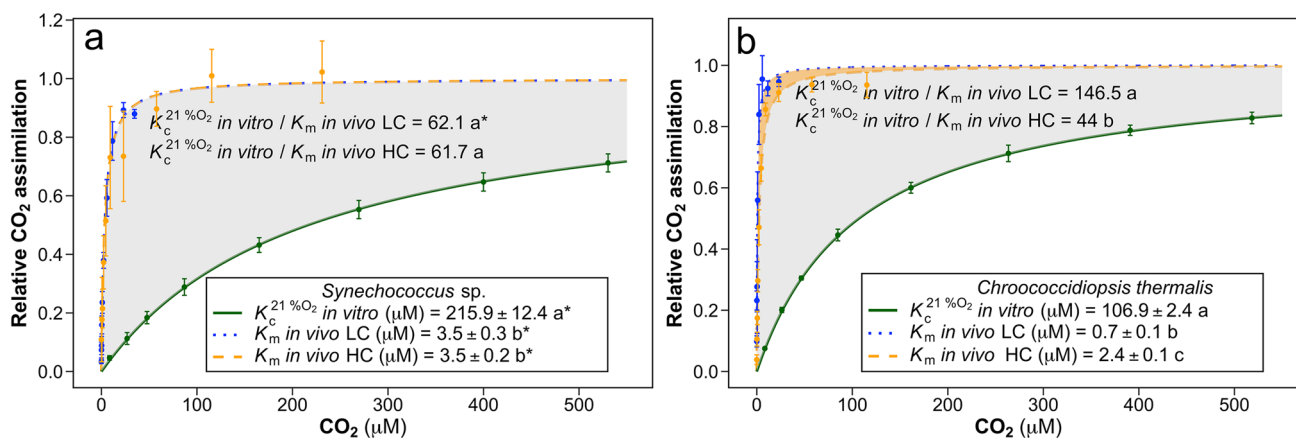
Fig. 3 Rubisco in vitro CO_2 assimilation under 21% O_2 (green line), photosynthetic in vivo CO_2 assimilation of ambient air grown cells (blue dotted line; LC) and photosynthetic in vivo CO_2 assimilation of 2.5% CO_2 grown cells (orange dashed line, HC) from **a** *Synechococcus* sp. PCC6301 and **b** *Chroococcidiopsisthermalis* KOMAREK 1964/111. The maximum Rubisco and photosynthetic CO_2 assimilation rates were standardized to 1 in both plots. The ratio between the Rubisco in vitro Michaelis–Menten semi-saturation constant for CO_2 under 21% O_2 ($K_c^{21\%O_2}$) and the photosynthetic in vivo Michaelis–Menten semi-saturation constant for CO_2 from either cells grown under ambient air ($K_{m\ in\ vivo}$ LC) or cells grown under 2.5% CO_2 ($K_{m\ in\ vivo}$ HC) indicates the CCM effectiveness. Different letters denote significant differences among treatments, and the asterisk (*) indicates significant differences between the two analyzed species ($P < 0.05$, Kruskal–Wallis test followed by Bonferroni correction for $K_c^{21\%O_2}$, $K_{min\ vivo}$ LC and $K_{m\ in\ vivo}$ HC within species; and Student's *t* test for parametric data, or Mann–Whitney–Wilcoxon test for non-parametric data, to compare means between species). 3–6 replicates were used to calculate the mean values of the Rubisco in vitro measurements and 10 replicates were used for the photosynthetic in vivo measurements

Table 1 Percentages of inhibition of net photosynthesis after the addition of the inhibitors acetazolamide (AZ), ethoxyzolamide (EZ) and 4,4′-diisothiocyanatostilbene-2,2′-disulfonate (DIDS) in *Synechococcus* sp. PCC6301 and *Chroococcidiopsis thermalis* KOMAREK 1964/111, both grown under ambient air (0.04% CO_2, LC) or 2.5% CO_2—enriched air (HC). Values are means ± standard deviations of 10 replicates

Species	CO_2 treatment	% inhibition AZ	% inhibition EZ	% inhibition DIDS
Synechococcus sp.	LC	11.7 ± 5.9 a	51.4 ± 6.7 ab*#	20.2 ± 8.1 a*
Synechococcus sp.	HC	23.5 ± 9.3 b*	46.8 ± 12.1 b*#	44.3 ± 7.4 b*
C. thermalis	LC	20.3 ± 5.0 ab*	65.6 ± 14.9 a*#	6.1 ± 2.3 c
C. thermalis	HC	35.4 ± 10.7 c*	86.9 ± 17.7 c*#	19.3 ± 5.6 a*

Different letters denote significant differences among strains and CO_2 treatments ($P < 0.05$, two-way ANOVA followed by Tukey's test or Kruskal–Wallis test followed with Bonferroni correction for non-parametric data). Asterisk (*) indicates a significant inhibition of the net photosynthetic rate ($P < 0.05$, Student's *t* test or Mann–Whitney–Wilcoxon test for non-parametric data). Hash (#) indicates significant differences between the net photosynthetic rate under AZ and that under EZ ($P < 0.05$, Student's *t* test or Mann–Whitney–Wilcoxon test for non-parametric data)

## In vivo photosynthetic affinity for CO_2 and CCM effectiveness

When comparing the two species grown under LC, *C. thermalis* presented a fivefold higher in vivo photosynthetic affinity for CO_2 than *Synechococcus* sp. (i.e. fivefold lower $K_{m\ in\ vivo}$, with values of 0.7 μM and 3.5 μM, respectively; Fig. 3). *Synechococcus* sp. did not change its $K_{m\ in\ vivo}$ between LC and HC-grown cells, whereas *C. thermalis* presented a more than threefold lower in vivo photosynthetic affinity for CO_2 when grown under HC than under LC ($K_{m\ in\ vivo}$ of 2.4 and 0.7 μM, respectively).

The effectiveness to concentrate CO_2 around Rubisco active sites from the CCM machinery was assessed by comparing the in vivo photosynthetic response to CO_2 with the in vitro Rubisco fixation response to CO_2 under 21% O_2 (Fig. 3 and Supplementary Fig. 1), through the ratio between $K_c^{21\%\ O_2}$ and $K_{m\ in\ vivo}$. CCM effectiveness in *C. thermalis* grown under LC was more than twofold higher than that found in *Synechococcus* sp. grown under LC ($K_c^{21\%\ O_2}/K_{m\ in\ vivo}$ ratio of 146.5 μM μM^{-1} and 62.1 μM μM^{-1}, respectively; Fig. 3). CCM effectiveness in *Synechococcus* sp. remained unvaried between the two CO_2 treatments. By contrast, CCM effectiveness in *C. thermalis* grown under HC was more than threefold lower than that found under LC (ratio $K_c^{21\%\ O_2}/K_{m\ in\ vivo}$ ratio of 44 μM μM^{-1} and 146.5 μM μM^{-1}, respectively).

Total Rubisco content and carbon isotopic fractionation

The percentage of Rubisco per total soluble protein (TSP) was invariable between CO_2 treatments in *C. thermalis*,
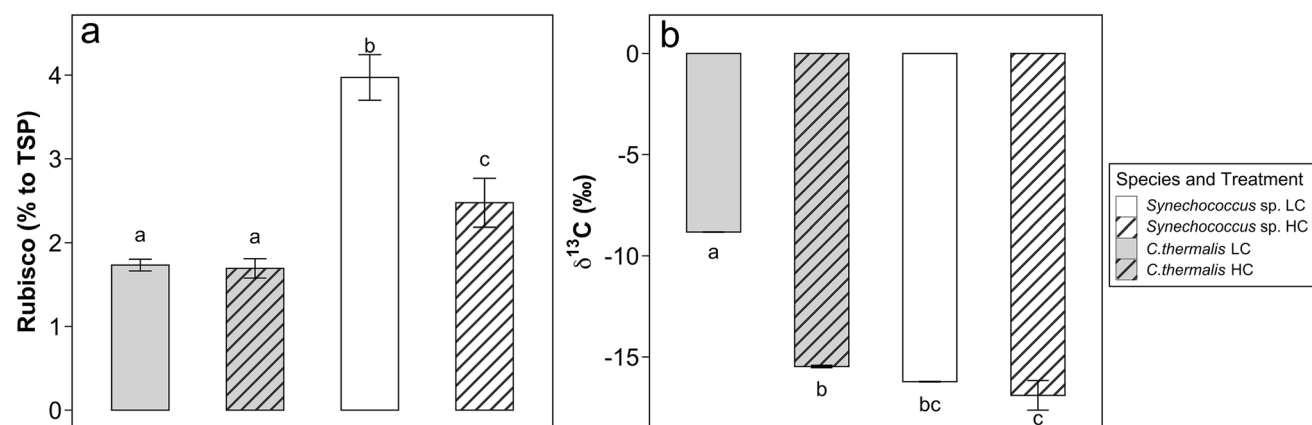
Fig. 4 **a** Percentage of Total Soluble Protein (TSP) that corresponds to Rubisco; **b** Cell ^{13}C isotopic discrimination (δ^{13}C). Values are means ± SD. White color corresponds to *Chroococcidiopsis thermalis* KOMAREK 1964/111 and grey color corresponds to *Synechococcus* sp. PCC6301. The line pattern refers to 2.5% CO_2—enriched air grown cells (HC) and the empty pattern to ambient air grown cells (0.04% CO_2, LC). Different letters denote significant differences among strains and CO_2 treatments ($P < 0.05$, two-way ANOVA followed by Tukey's test or Kruskal–Wallis test followed with Bonferroni correction for non-parametric data). 3 replicates were used to calculate the % of Rubisco to TSP and 4–7 replicates to calculate δ^{13}C

averaging 1.7% of TSP (Fig. 4a, Supplementary Fig. 2). On the contrary, the percentage of TSP being Rubisco in *Synechococcus* sp. grown under LC was significantly higher than that under HC (4% and 2.5%, respectively). Overall, 1.5-fold higher values of Rubisco per TSP were observed in *Synechococcus* sp. in comparison with *C. thermalis*, when both species were grown under LC (Fig. 4a).

Carbon isotopic fractionation of the biomass ($\delta^{13}C$) was significantly less negative in *C. thermalis* ($\delta^{13}C$ of − 8.8 ‰) than in *Synechococcus* sp. under LC (− 16.2 ‰, Fig. 4b), suggesting a stronger bicarbonate use in the former. $\delta^{13}C$ of *Synechococcus* sp. was invariable between the two CO_2 treatments. On the contrary, $\delta^{13}C$ of *C. thermalis* becomes 1.7-fold more negative when grown under HC relative to the value found under LC, acquiring similar values as in *Synechococcus* sp. ($\delta^{13}C$ of − 15.47 ‰).

Rubisco gross assimilation modeling

Modeled Rubisco-limited gross assimilation rate (A_{Rub}) at 25 °C in *C. thermalis* was higher than that of *Synechococcus* sp. at the whole range of CO_2 partial pressure at the Rubisco active sites (C_c) tested, and higher than *T. aestivum* at C_c above 700 µbar (Fig. 5a, b). Cyanobacterial A_{Rub} saturated at much higher C_c than *T. aestivum*, but A_{Rub} from *C. thermalis* saturated at lower C_c than *Synechococcus* sp.

Anatomical differences between *C. thermalis* and *Synechococcus* sp.

Cell area (Table 2 and Fig. 6) did not differ between the two CO_2 treatments in *Synechococcus* sp. (1.6 µm^2 in LC and 1.7 µm^2 in HC), while in *C. thermalis*, it was higher in
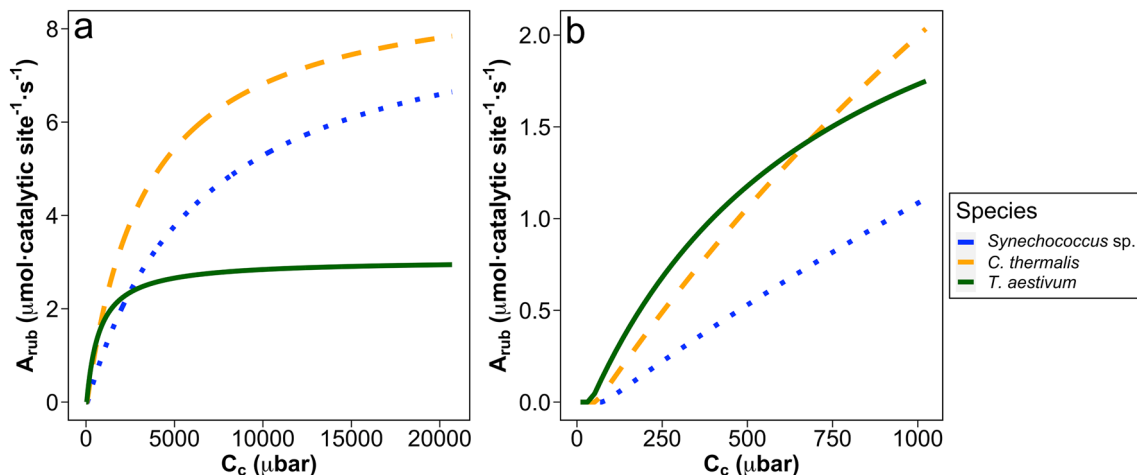
Fig. 5 **a** Modeled Rubisco gross assimilation rate (A_{Rub}) at 25 °C at varying CO_2 partial pressure at the Rubisco active sites (C_c) of *Synechococcus* sp. PCC 6301 (blue dotted line), *Chroococcidiopsis ther-* *malis* KOMAREK 1964/111 (orange dashed line) and *Triticum aestivum* (green line), and **b** Previous graph zoomed in at a C_c ranging from 0 to 900 µbar

Table 2 Transmission electron microscopy image characterization of cell area, number of carboxysomes per cell, total carboxysome area per cell, average area of each carboxysome and percentage of the cell area occupied by carboxysomes, in *Synechococcus* sp. PCC6301 and *Chroococcidiopsis thermalis* KOMAREK 1964/111 grown either under ambient air (0.04% CO_2, LC) or 2.5% CO_2—enriched air (HC)

Species	CO_2 treatment	Cell area (µm^2)	No. carboxysomes per cell	Total carboxysome area per cell (µm^2)	Average area of each carboxysome (µm^2)	% carboxysome area
Synechococcus sp.	LC	1.6 ± 0.4 a	1.3 ± 0.5 a	0.09 ± 0.04 a	0.08 ± 0.04 a	6.1 ± 3.3 a
Synechococcus sp.	HC	1.7 ± 0.4 a	1.1 ± 0.4 a	0.08 ± 0.04 a	0.07 ± 0.04 a	4.7 ± 2.8 a
C. thermalis	LC	3.8 ± 1.2 b	2.9 ± 1.1 b	0.08 ± 0.03 a	0.03 ± 0.01 b	2.3 ± 1.0 b
C. thermalis	HC	5.4 ± 1.6 c	2.5 ± 1.1 b	0.14 ± 0.08 b	0.06 ± 0.02 a	2.7 ± 1.2 b

Values are means ± standard deviations of 30 measured cells per species and treatment. Different letters denote significant differences among different strains and CO_2 treatments ($P < 0.05$, two-way ANOVA followed by Tukey's test or Kruskal–Wallis test followed with Bonferroni correction for non-parametric data)
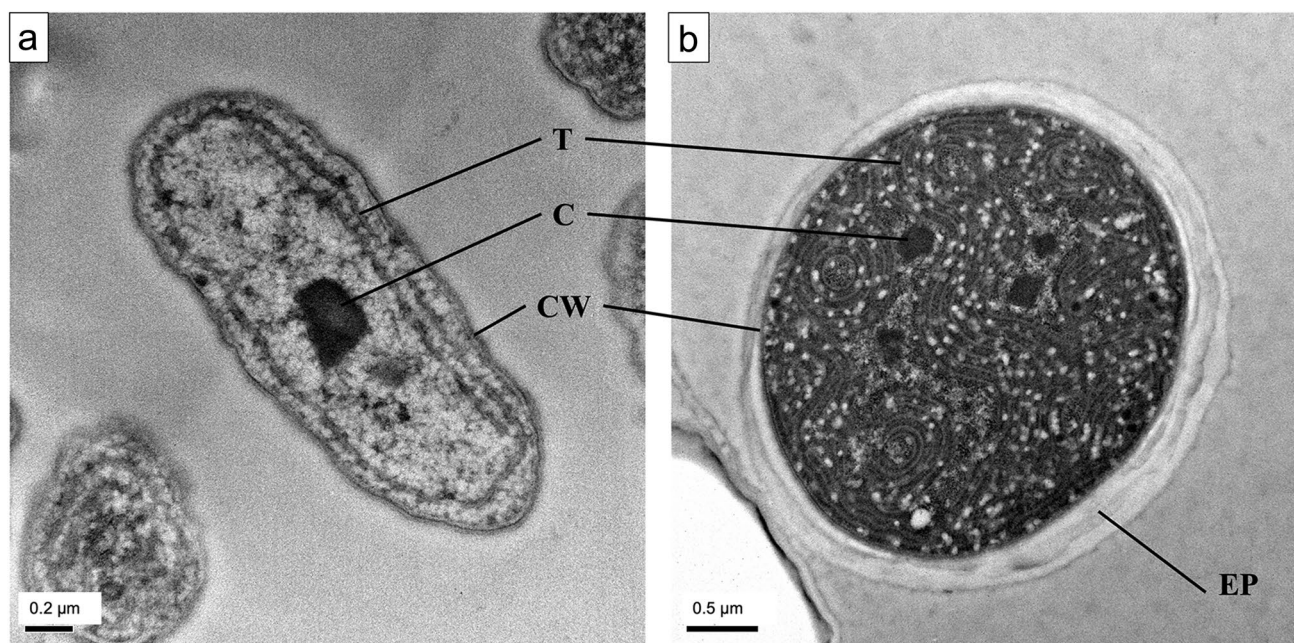
Fig. 6 Transmission electron microscope images of **a** *Synechococcus* sp. PCC6301 and **b** *Chroococcidiopsis thermalis* KOMAREK 1964/111. *EP* exopolysaccharide shell, *CW* cell wall, *C* carboxysome, *T* thylakoid membrane. Scale bars are 0.2 µm for *Synechococcus* sp. and 0.5 µm for *C. thermalis*

HC-grown cells as compared to LC-grown cells (5.4 µm^2 and 3.8 µm^2, respectively). The number of carboxysomes per cell was more than twofold higher in *C. thermalis* than in *Synechococcus* sp. but did not differ between the two CO_2 treatments within each species (Table 2). The total carboxysome area per cell was independent of the CO_2 treatment in *Synechococcus* sp., whereas in *C. thermalis,* it was almost double in HC than in LC-grown cells (0.14 and 0.08 µm^2, respectively). Therefore, the average area for one carboxysome in *C. thermalis* under HC was also twofold higher than under LC. Finally, the percentage of the cell area occupied by carboxysomes (% carboxysome area, Table 2) was 2 to threefold higher in *Synechococcus* sp. than in *C. thermalis*, not being affected by the CO_2 treatment in any of the species.

Discussion

Remarkable Rubisco kinetic performance in *C. thermalis* within Cyanobacteria

The present results show a large variability in Rubisco kinetics within Cyanobacteria, consistent with what has been shown in recent reviews focused on Rubisco evolution in photosynthetic organisms (Bathellier et al. 2018; Flamholz et al. 2019; Iñiguez et al. 2020). The following message of this finding is that more diverse and efficient Rubiscos can be discovered in barely explored groups, such as Cyanobacteria.

Chroococcidiopsis thermalis showed the highest values for Rubisco $S_{c/o}$ and carboxylation efficiency (k_{cat}^c/K_c) ever obtained for a cyanobacterium to date. In general, cyanobacterial Rubisco kinetic traits are characterized by low $S_{c/o}$ values, along with high k_{cat}^c, K_c and K_o (Iñiguez et al. 2020), which suggest that the Rubisco from Cyanobacteria have evolved in an intracellular CO_2-enriched environment driven by effective CCMs (Flamholz et al. 2019). However, such a high $S_{c/o}$ value of *C. thermalis*, which resembles those found in pyrenoid-containing green algae or even those from some vascular plants provided with CCMs (Kubien et al. 2008; Sharwood et al. 2016; Capó-Bauçà et al. 2022b), is the result of a higher affinity for CO_2 and lower affinity for O_2 in comparison to other cyanobacterial strains. This suggests that Rubisco evolution in this phylogenetic group is not strictly constrained, and improved $S_{c/o}$ is still compatible with high k_{cat}^c values, as previously discussed by Cummins et al. (2018) and Bouvier et al. (2021). The combination of *C. thermalis* Rubisco kinetic traits could be an adaptive mechanism that allows this species to deal with extremely low environmental CO_2 concentrations (i.e. at high water temperatures or under desiccation). Moreover, the concentration of Rubisco in *C. thermalis* was insensible to the CO_2 treatment, contrary to the response observed for *Synechococcus* sp. in our study and for other cyanobacterial strains in other works (Sengupta et al. 2019; Garcia et al.

2021). This indicates that the amount of Rubisco in *C. thermalis* is not involved in the process of acclimation to different environmental CO_2 concentrations. Hence, Rubisco from *C. thermalis* has evolved towards an enhancement of CO_2 fixation rates regardless of the environmental CO_2 concentrations. Indeed, potential Rubisco gross assimilation (A_{Rub}) from *C. thermalis* exhibited higher values than *Synechococcus* sp. for the whole range of C_c tested (Fig. 5a).

Co-evolution of Rubisco and CCMs in *C. thermalis* and *Synechococcus* sp.

There are three main components of the cyanobacterial CCM machinery: CAs, carboxysomes, and inorganic carbon (C_i) transporters (Badger et al. 2002). The main C_i transporters are HCO_3^- transporters and CO_2 uptake components including NDH-1 dehydrogenase complex (Woodger et al. 2005) whereas CAs can possess an extracellular or intracellular localization. HCO_3^- transporters are involved in the active transport of HCO_3^- through the plasma membrane, while the NDH-1 complex (CO_2 uptake components) catalyzes the hydration of CO_2 to HCO_3^- inside the cell (Badger et al. 2002). In this sense, the effects of the inhibitors of CCM components (such as AZ, EZ and DIDS) on the net photosynthetic rates used in the present study for both cyanobacterial strains were similar to those recorded in other studies with mat-forming cyanobacterial strains (Carrasco et al. 2008) and were not reduced by the enriched CO_2 treatment. However, some differences in the CCM components between the two species were detected, as the anion exchange inhibitor DIDS produced a significantly higher net photosynthetic inhibition in *Synechococcus* sp. than in *C. thermalis* for both CO_2 treatments. The remarkable high EZ inhibition and the relatively low AZ inhibition of net photosynthesis from *C. thermalis* indicate an important role of internal CAs in its CCM. Therefore, these results suggest that *C. thermalis* might possess an elevated activity of either other type/s of bicarbonate transporter/s not inhibited by DIDS and/or CO_2 uptake components such as the NDH-1 dehydrogenase complex to supply bicarbonate to the carboxysomes.

Highly effective CCMs were detected in both species since the ratio $K_c^{21\ \%\ O_2}/K_{m\ in\ vivo}$ was greater than 2.5, as proposed by Raven et al. (2017) (Fig. 3). However, the CCM effectiveness of *C. thermalis* under LC was among the highest ever reported for a cyanobacterium, concentrating CO_2 around Rubisco active sites more than 140 times the external CO_2 levels, 2.3-fold higher than *Synechococcus* sp. PCC6301.

Previous studies with different model cyanobacterial strains reported much lower in vivo photosynthetic affinity for CO_2 (i.e. higher K_m in vivo than *C. thermalis* when grown under similar enriched CO_2 levels (Whitehead et al. 2014). Thus, *C. thermalis* not only evolved improved

Rubisco carboxylation kinetics but also stronger CCMs than other cyanobacterial strains. This response does not follow the inverse relationship between Rubisco carboxylation efficiency and CCM effectiveness previously observed in other photosynthetic groups (Capó-Bauçà et al. 2022a, b) and might indicate that co-evolution between CCMs and Rubisco kinetics in some cyanobacteria is not as constrained as in other phylogenetic groups.

Inhabiting warm-desertic areas, *C. thermalis* has to face extremely high temperatures up to 68ºC (Hindák et al. 2013) that led to a strong limitation in CO_2 availability (i.e. CO_2 solubility decreases at higher temperatures). In addition, *C. thermalis* produces a scytonemin rich exopolysaccharide shell to resist desiccation (Vítek et al. 2014; Casero et al. 2021) that might exacerbate CO_2 limitation through a strong reduction in CO_2 diffusion from the extracellular medium to Rubisco active sites. Therefore, the development of more effective CCMs in combination with more efficient Rubisco carboxylation kinetics could have contributed to the adaptation of *C. thermalis* to these extreme environments. Since the operation of cyanobacterial CCM depends on the velocity of active HCO_3^- transport and the permeability of the carboxysome to CO_2 and HCO_3^- (Mangan and Brenner 2014), these processes should be explored in *C. thermalis* in future studies in comparison with model cyanobacterial species to identify the main molecular adaptations that allow this cyanobacterium to possess one of the most effective CCMs ever reported.

In addition, indirect proxies used to detect CCM activity (effect of CCMs inhibitors on net photosynthesis, carbon isotope discrimination, the ratio between the semi-saturation constant for CO_2 in vitro and in vivo, and the morpho-anatomical carboxysome analysis) confirmed the acclimatory capacity of the CCM machinery in *C. thermalis* to respond to changes in environmental CO_2 concentrations. CCM effectiveness in *C. thermalis* was significantly reduced when grown under HC (since the in vivo photosynthetic semi-saturation constant for CO_2 was more than threefold higher in HC-grown cells relative to LC-grown cells). This fact, together with a more negative $\delta^{13}C$ under HC, indicates a downregulation of CCM machinery in *C. thermalis* caused by the increase in environmental CO_2 concentration. The CCM downregulation could be a mechanism to save energy for other vital processes (Beardall and Giordano 2002) while maintaining similar net photosynthetic rates, as previously observed in other aquatic photosynthetic organisms (Gordillo et al. 2001; Iñiguez et al. 2016; Ma and Wang 2021). Such downregulation was not observed in *Synechococcus* sp., where CCM effectiveness and $\delta^{13}C$ remained constant independently of the CO_2 treatment applied, and, as a result, the net photosynthetic rate was almost double under HC despite the decrease in Rubisco quantity per TSP. This might be due to a faster acclimation of *C. thermalis* CCMs than

Synechococcus sp. CCMs to changes in environmental CO_2 concentration, which may allow the former to thrive under harsh conditions of high temperature and water scarcity.

Potential crop yield improvement by the introduction of cyanobacterial carbon utilization mechanisms

Increasing crop yield is a must to face the food needs of the rising population (Ray et al. 2013) since the decreased arable land and climate change impact on crops represent important risks for plant production (Long et al. 2015). Bioengineering approaches for photosynthesis optimization have largely demonstrated the potential for enhancing crop yield, for example by enhancing Rubisco carboxylation capacity (reviewed by Iñiguez et al. (2021)). Several attempts have tried to enhance photosynthetic rates from crops by introducing some basic CCM components and Rubisco from Cyanobacteria. For example, Lin et al. (2014) successfully transformed tobacco plants by expressing *Synechococcus elongatus* PCC 7942 Rubisco with an internal carboxysome protein (CcmM35) producing functional macromolecular complexes. In addition, Long et al. (2018) reconstituted simplified carboxysomes with a minimum set of genes from the genus *Cyanobium* into tobacco chloroplast that were able to encapsulate the cyanobacterial Rubisco. However, none of the transformed tobacco lines expressing simplified carboxysome-like structures were still able to grow equally or faster than wild-type plants. Directions towards fully functional cyanobacterial CCM expression in C_3 plant chloroplasts go through targeting functional bicarbonate transporter proteins into the chloroplast membranes (Rolland et al. 2016), a hit that might be achievable soon. Here, we have discovered the most CO_2-specific and efficient cyanobacterial Rubisco ever reported, which represents a potential candidate for bioengineering crop species to increase crop yield in combination with cyanobacterial CCM expression, as the potential capacity for CO_2 assimilation of *C. thermalis* Rubisco is significantly higher than those from *Synechococcus* sp. PCC6301 and other analyzed cyanobacterial species.

Conclusions

The present results represent the first complete characterization of inorganic carbon utilization mechanisms in a non-model cyanobacterium, as in vivo CO_2 assimilation data was complemented with in vitro Rubisco measurements, Rubisco content, ^{13}C isotopic discrimination, and the use of CCM inhibitors. This has allowed us to inquire into the inorganic carbon utilization adaptations of a polyextremophilic cyanobacterium. The main highlights of the study are the discovery in *C. thermalis* of the highest values of Rubisco specificity for CO_2 over O_2 and catalytic carboxylation efficiency ever obtained for Cyanobacteria, together with the most effective CO_2-concentrating mechanisms. This allows *C. thermalis* to thrive under CO_2-limited environments such as elevated temperatures and/or desertic areas. Overall, further exploration of Rubisco kinetics and CCM operation from underrepresented phylogenetic groups is needed to discover highly valuable mechanisms for biotechnological applications.

Declarations

References

Andersson I, Backlund A (2008) Structure and function of Rubisco. Plant Physiol Biochem 46:275–291. https://doi.org/10.1016/j.plaphy.2008.01.001

Badger MR, Andrews TJ (1987) CO-Evolution of Rubisco and CO_2 concentrating mechanisms. In: Progress in photosynthesis research, pp 601–609

Badger MR, Hanson D, Price GD (2002) Evolution and diversity of CO_2 concentrating mechanisms in cyanobacteria. Funct Plant Biol 29:161–173. https://doi.org/10.1071/pp01213

Basu S, Mackey KRM (2022) Effect of rising temperature and carbon dioxide on the growth, photophysiology, and elemental ratios of marine *Synechococcus*: a multistressor approach. Sustainability 14:9508. https://doi.org/10.3390/su14159508

Bathellier C, Tcherkez G, Lorimer GH, Farquhar GD (2018) Rubisco is not really so bad. Plant Cell Environ 41:705–716. https://doi.org/10.1111/pce.13149

Bauwe H, Hagemann M, Fernie AR (2010) Photorespiration: players, partners and origin. Trends Plant Sci 15:330–336. https://doi.org/10.1016/j.tplants.2010.03.006

Bauwe H, Hagemann M, Kern R, Timm S (2012) Photorespiration has a dual origin and manifold links to central metabolism. Curr Opin Plant Biol 15:269–275. https://doi.org/10.1016/j.pbi.2012.01.008

Beardall J, Giordano M (2002) Ecological implications of algal CCMs and their regulation. Funct Plant Biol 29:335–347. https://doi.org/10.1071/PP01195

Billi D, Viaggiu E, Cockell CS et al (2011) Damage escape and repair in dried *Chroococcidiopsis* spp. from hot and cold deserts exposed to simulated space and martian conditions. Astrobiology 11:65–73. https://doi.org/10.1089/ast.2009.0430

Blank CE (2013) Origin and early evolution of photosynthetic eukaryotes in freshwater environments: reinterpreting proterozoic paleobiology and biogeochemical processes in light of trait evolution. J Phycol 49:1040–1055. https://doi.org/10.1111/jpy.12111

Blayney MJ, Whitney SM, Beck JL (2011) NanoESI mass spectrometry of Rubisco and Rubisco activase structures and their interactions with nucleotides and sugar phosphates. J Am Soc Mass Spectrom 22:1588–1601. https://doi.org/10.1007/s13361-011-0187-8

Bouvier JW, Emms DM, Rhodes T et al (2021) Rubisco adaptation is more limited by phylogenetic constraint than by catalytic trade-off. Mol Biol Evol 38:2880–2896. https://doi.org/10.1093/molbev/msab079

Bradford MM (1976) A rapid and sensitive method for the quantitation of microgram quantities of protein utilizing the principle of pretein-dye binding. Anal Biochem 72:248–254

Capó-Bauçà S, Font-Carrascosa M, Ribas-Carbó M et al (2020) Biochemical and mesophyll diffusional limits to photosynthesis are determined by prey and root nutrient uptake in the carnivorous pitcher plant Nepenthes × ventrata. Ann Bot 126:25–37. https://doi.org/10.1093/aob/mcaa041

Capó-Bauçà S, Galmés J, Aguiló-Nicolau P et al (2022a) Carbon assimilation in upper subtidal macroalgae is determined by an inverse correlation between Rubisco carboxylation efficiency and CO_2 concentrating mechanism effectiveness. New Phytol. https://doi.org/10.1111/nph.18623

Capó-Bauçà S, Iñiguez C, Aguiló-Nicolau P, Galmés J (2022b) Correlative adaptation between Rubisco and CO_2-concentrating mechanisms in seagrasses. Nat Plants 8:706–716. https://doi.org/10.1038/s41477-022-01171-5

Carrasco M, Mercado JM, Niell FX (2008) Diversity of inorganic carbon acquisition mechanisms by intact microbial mats of *Microcoleus chthonoplastes* (Cyanobacteriae, Oscillatoriaceae). Physiol Plant 133:49–58. https://doi.org/10.1111/j.1399-3054.2007.01032.x

Casero MC, Ascaso C, Quesada A et al (2021) Response of endolithic *Chroococcidiopsis* strains from the Polyextreme Atacama desert to light radiation. Front Microbiol 11:1–13. https://doi.org/10.3389/fmicb.2020.614875

Cumbers J, Rothschild LJ (2014) Salt tolerance and polyphyly in the cyanobacterium *Chroococcidiopsis* (Pleurocapsales). J Phycol 50:472–482. https://doi.org/10.1111/jpy.12169

Cummins PL, Kannappan B, Gready JE (2018) Directions for optimization of photosynthetic carbon fixation: Rubisco's efficiency may not be so constrained after all. Front Plant Sci 9:183. https://doi.org/10.3389/fpls.2018.00183

Dai W, Chen M, Myers C et al (2018) Visualizing individual RuBisCO and its assembly into carboxysomes in marine cyanobacteria by cryo-electron tomography. J Mol Biol 430:4156–4167. https://doi.org/10.1016/j.jmb.2018.08.013.Visualizing

Davidi D, Shamshoum M, Guo Z et al (2020) Highly active rubiscos discovered by systematic interrogation of natural sequence diversity. EMBO J 39:1–11. https://doi.org/10.15252/embj.2019104081

Dismukes GC, Klimov VV, Baranov SV et al (2001) The origin of atmospheric oxygen on Earth: the innovation of oxygenic photosynthesis. Proc Natl Acad Sci USA 98:2170–2175. https://doi.org/10.1073/pnas.061514798

Ellis RJ (1979) The most abundant protein in the world. Trends Biochem Sci 4:241–244. https://doi.org/10.1016/0968-0004(79)90212-3

Espie GS, Kimber MS (2011) Carboxysomes: cyanobacterial RubisCO comes in small packages. Photosynth Res 109:7–20. https://doi.org/10.1007/s11120-011-9656-y

Farquhar GD, Caemmerer S, Berry JA (1980) A biochemical model of photosynthetic CO_2 assimilation in leaves of C_3 species. Planta 149:78–90

Flamholz A, Shih PM (2020) Cell biology of photosynthesis over geologic time. Curr Biol 30:R490–R494. https://doi.org/10.1016/j.cub.2020.01.076

Flamholz AI, Prywes N, Moran U et al (2019) Revisiting trade-offs between Rubisco kinetic parameters. Biochemistry 58:3365–3376. https://doi.org/10.1021/acs.biochem.9b00237

Galmés J, Conesa MÀ, Díaz-Espejo A et al (2014a) Rubisco catalytic properties optimized for present and future climatic conditions. Plant Sci 226:61–70. https://doi.org/10.1016/j.plantsci.2014.01.008

Galmés J, Kapralov MV, Andralojc PJ et al (2014b) Expanding knowledge of the Rubisco kinetics variability in plant species: environmental and evolutionary trends. Plant Cell Environ 37:1989–2001. https://doi.org/10.1111/pce.12335

Galmés J, Hermida-Carrera C, Laanisto L, Niinemets Ü (2016) A compendium of temperature responses of Rubisco kinetic traits: variability among and within photosynthetic groups and impacts on photosynthesis modeling. J Exp Bot 67:5067–5091. https://doi.org/10.1093/jxb/erw267

Garcia AK, Kedzior M, Taton A et al (2021) System-level effects of CO_2 and RuBisCO concentration on carbon isotope fractionation. bioRxiv 2021.04.20.440233

Giordano M, Beardall J, Raven JA (2005) CO_2 concentrating mechanisms in algae: mechanisms, environmental modulation, and evolution. Annu Rev Plant Biol 56:99–131. https://doi.org/10.1146/annurev.arplant.56.032604.144052

Gordillo FJL, Niell FX, Figueroa FL (2001) Non-photosynthetic enhancement of growth by high CO_2 level in the nitrophilic seaweed *Ulva rigida* C. Agardh (Chlorophyta). Planta 213:64–70. https://doi.org/10.1007/s004250000468

Hamilton TL (2019) The trouble with oxygen: the ecophysiology of extant phototrophs and implications for the evolution of oxygenic photosynthesis. Free Radic Biol Med 140:233–249. https://doi.org/10.1016/j.freeradbiomed.2019.05.003

Hindák F, Kvíderová J, Lukavský J (2013) Growth characteristics of selected thermophilic strains of cyanobacteria using crossed gradients of temperature and light. Biology 68:830–837. https://doi.org/10.2478/s11756-013-0215-1

Iñiguez C, Carmona R, Lorenzo MR et al (2016) Increased temperature, rather than elevated CO_2, modulates the carbon assimilation of the Arctic kelps *Saccharina latissima* and *Laminaria solidungula*. Mar Biol 163:1–18. https://doi.org/10.1007/s00227-016-3024-6

Iñiguez C, Capó-Bauçà S, Niinemets Ü et al (2020) Evolutionary trends in RuBisCO kinetics and their co-evolution with CO_2 concentrating mechanisms. Plant J 101:897–918. https://doi.org/10.1111/tpj.14643

Iñiguez C, Aguiló-Nicolau P, Galmés J (2021) Improving photosynthesis through the enhancement of Rubisco carboxylation capacity. Biochem Soc Trans 49:2007–2019. https://doi.org/10.1042/BST20201056

Jordan DB, Ogren WL (1983) Species variation in kinetic properties of ribulose 1,5-bisphosphate carboxylase/oxygenase. Arch Biochem Biophys 227:425–433. https://doi.org/10.1016/0003-9861(83)90472-1

Kane HJ, Viil J, Entsch B et al (1994) An improved method for measuring the CO_2/O_2 specificity of ribulosebisphosphatte carboxylase-oxygenase. Aust J Plant Physiol 21:449–461. https://doi.org/10.1071/PP9940449

Knoll AH (2008) Cyanobacteria and Earth history. Cyanobacteria Mol Biol Genomics Evol 1–20

Kubien DS, Whitney SM, Moore PV, Jesson LK (2008) The biochemistry of Rubisco in Flaveria. J Exp Bot 59:1767–1777. https://doi.org/10.1093/jxb/erm283

Lin MT, Occhialini A, Andralojc PJ et al (2014) A faster Rubisco with potential to increase photosynthesis in crops. Nature 513:547–550. https://doi.org/10.1038/nature13776

Long SP, Marshall-Colon A, Zhu XG (2015) Meeting the global food demand of the future by engineering crop photosynthesis and yield potential. Cell 161:56–66. https://doi.org/10.1016/j.cell.2015.03.019

Long BM, Hee WY, Sharwood RE et al (2018) Carboxysome encapsulation of the CO_2-fixing enzyme Rubisco in tobacco chloroplasts. Nat Commun 9:1–14. https://doi.org/10.1038/s41467-018-06044-0

Losh JL, Young JN, Morel FMM (2013) Rubisco is a small fraction of total protein in marine phytoplankton. New Phytol 198:52–58. https://doi.org/10.1111/nph.12143

Ma J, Wang P (2021) Effects of rising atmospheric CO_2 levels on physiological response of cyanobacteria and cyanobacterial bloom development: a review. Sci Total Environ 754:141889. https://doi.org/10.1016/j.scitotenv.2020.141889

Mangan N, Brenner M (2014) Systems analysis of the CO_2 concentrating mechanism in cyanobacteria. elife 2014:1–17. https://doi.org/10.7554/eLife.02043

Mangan NM, Flamholz A, Hood RD et al (2016) PH determines the energetic efficiency of the cyanobacterial CO_2 concentrating mechanism. Proc Natl Acad Sci USA 113:E5354–E5362. https://doi.org/10.1073/pnas.1525145113

Rae BD, Long BM, Whitehead LF et al (2013) Cyanobacterial carboxysomes: microcompartments that facilitate CO_2 fixation. J Mol Microbiol Biotechnol 23:300–307. https://doi.org/10.1159/000351342

Raven JA (2013) Rubisco: still the most abundant protein of Earth? New Phytol 198:1–3. https://doi.org/10.1111/nph.12197

Raven JA, Beardall J, Sánchez-Baracaldo P (2017) The possible evolution and future of CO_2-concentrating mechanisms. J Exp Bot 68:3701–3716. https://doi.org/10.1093/jxb/erx110

Ray DK, Mueller ND, West PC, Foley JA (2013) Yield trends are insufficient to double global crop production by 2050. PLoS ONE 8:e66428. https://doi.org/10.1371/journal.pone.0066428

Rolland V, Badger MR, Price GD (2016) Redirecting the cyanobacterial bicarbonate transporters bica and sbta to the chloroplast envelope: soluble and membrane cargos need different chloroplast targeting signals in plants. Front Plant Sci 7:1–19. https://doi.org/10.3389/fpls.2016.00185

Ruuska S, Andrews TJ, Badger MR et al (1998) The interplay between limiting processes in C3 photosynthesis studied by rapid-response gas exchange using transgenic tobacco impaired in photosynthesis Sari. Aust J Plant Physiol 25:859–870. https://doi.org/10.1007/s13361-011-0187-8

Sánchez-Baracaldo P, Bianchini G, Wilson JD, Knoll AH (2022) Cyanobacteria and biogeochemical cycles through Earth history. Trends Microbiol 30:143–157. https://doi.org/10.1016/j.tim.2021.05.008

Schirrmeister BE, Sanchez-Baracaldo P, Wacey D (2016) Cyanobacterial evolution during the Precambrian. Int J Astrobiol 15:187–204. https://doi.org/10.1017/S1473550415000579

Sengupta A, Sunder AV, Sohoni SV, Wangikar PP (2019) Fine-tuning native promoters of *Synechococcus elongatus* PCC 7942 to develop a synthetic toolbox for heterologous protein expression. ACS Synth Biol 8:1219–1223. https://doi.org/10.1021/acssynbio.9b00066

Sharwood RE, Ghannoum O, Whitney SM (2016) Prospects for improving CO_2 fixation in C3-crops through understanding C4-Rubisco biogenesis and catalytic diversity. Curr Opin Plant Biol 31:135–142. https://doi.org/10.1016/j.pbi.2016.04.002

Shih PM, Occhialini A, Cameron JC et al (2016) Biochemical characterization of predicted Precambrian RuBisCO. Nat Commun 7:10382. https://doi.org/10.1038/ncomms10382

Spreitzer RJ, Salvucci ME (2002) Rubisco: structure, regulatory interactions, and possibilities for a better enzyme. Annu Rev Plant Biol 53:449–475. https://doi.org/10.1146/annurev.arplant.53.100301.135233

Staub R (1961) Ernährungsphysiologisch- autökologische Untersuchungen an der planktischen Blaualge Oscillatoria rubescens DC. Schweizerische Zeitschrift für Hydrol 23:82–198. https://doi.org/10.3929/ethz-a-000092335

Tcherkez GG, Bathellier C, Farquhar GD, Lorimer GH (2018) Commentary: directions for optimization of photosynthetic carbon fixation: Rubisco's efficiency may not be so constrained after all. Front Plant Sci 9:1–4. https://doi.org/10.3389/fpls.2018.00929

Tomitani A, Knoll AH, Cavanaugh CM, Ohno T (2006) The evolutionary diversification of cyanobacteria: molecular-phylogenetic and paleontological perspectives. Proc Natl Acad Sci USA 103:5442–5447. https://doi.org/10.1073/pnas.0600999103

Vítek P, Jehlička J, Ascaso C et al (2014) Distribution of scytonemin in endolithic microbial communities from halite crusts in the hyper-arid zone of the Atacama Desert, Chile. FEMS Microbiol Ecol 90:351–366. https://doi.org/10.1111/1574-6941.12387

Whitehead L, Long BM, Dean Price G, Badger MR (2014) Comparing the in vivo function of α-carboxysomes and β-carboxysomes in two model cyanobacteria. Plant Physiol 165:398–411. https://doi.org/10.1104/pp.114.237941

Whitney SM, Baldet P, Hudson GS, John Andrews T (2001) Form I Rubiscos from non-green algae are expressed abundantly but not assembled in tobacco chloroplasts. Plant J 26:535–547. https://doi.org/10.1046/j.1365-313X.2001.01056.x

Wilson RH, Martin-Avila E, Conlan C, Whitney SM (2018) An improved *Escherichia coli* screen for Rubisco identifies a

protein-protein interface that can enhance CO_2-fixation kinetics. J Biol Chem 293:18–27. https://doi.org/10.1074/jbc.M117.810861

Woodger FJ, Badger MR, Price GD (2005) Sensing of inorganic carbon limitation in *Synechococcus* PCC7942 is correlated with the size of the internal inorganic carbon pool and involves oxygen. Plant Physiol 139:1959–1969. https://doi.org/10.1104/pp.105.069146

Xia LY, Jiang YL, Kong WW et al (2020) Molecular basis for the assembly of RuBisCO assisted by the chaperone Raf1. Nat Plants 6:708–717. https://doi.org/10.1038/s41477-020-0665-8

Young JN, Heureux AMC, Sharwood RE et al (2016) Large variation in the Rubisco kinetics of diatoms reveals diversity among their carbon-concentrating mechanisms. J Exp Bot 67:3445–3456. https://doi.org/10.1093/jxb/erw163